

Landslides (2020) 17:543–555
 DOI 10.1007/s10346-019-01297-2
 Received: 6 January 2019
 Accepted: 27 September 2019
 Published online: 15 November 2019
 © Springer-Verlag GmbH Germany
 part of Springer Nature 2019

Youkou Dong · Dong Wang · Lan Cui

Assessment of depth-averaged method in analysing runout of submarine landslide

Abstract Depth-averaged method (DAM) is one of the widely used numerical methods to back analyse the post-failure deposits of submarine landslides due to its high efficiency. However, its simplifications of the velocities along the thickness of the slide cannot capture complex behaviours such as shear band propagation. A novel non-averaged method, material point method (MPM), is used to validate the DAM analysis. The runout distances and morphologies of viscous debris flows predicted by the DAM and MPM are compared with those predicted by experiments and computational fluid dynamics analyses. The ranges of the shear strength, viscosity and sensitivity parameters are investigated to determine the feasibility of the DAM. The conventional DAM algorithm specialised for no-slip bases is enhanced to reproduce the phenomenon of block sliding of slides on frictional bases by considering the stability of the front and rear faces. Then, a spreading of horsts and grabens due to shear band propagation is presented with the MPM analysis. Two real cases of submarine landslides, Southern Mediterranean slide and Finneidfjord slide, were back-analysed with the DAM and MPM.

Keywords Depth-averaged method · Material point method · Submarine landslide · Runout · Morphology · Large deformation

Introduction

Submarine landslides are one of the most hazardous threat to the subsea infrastructure in oil and gas exploitation, which encompass a variety of subsea geological events with downslope movement of sediment masses bounded by distinct failure planes (Locat and Lee 2005; Highland and Peter 2008). Enormous volumes of sediments, a mixture of sands, clays and grains, can be transported by submarine landslides, which are two to three orders of magnitude larger than typical subaerial slides (Hampton et al. 1996). The velocity of a submarine landslide can be higher than 20 m/s and runout distance up to hundreds of kilometres before final deposition (Norem et al. 1990; Bryn et al. 2005; Leynaud et al. 2007). Analysing the runout process and evolution of morphologies of the rapid landslides is fundamental to quantitatively evaluate the vulnerable areas and the intensity of the disaster, hence benefits the hazard prevention strategies. As little information can be obtained on the unpredictable, infrequent and short-lived sliding processes, most of the present knowledge on submarine slides relies upon back-analysis of post-failure deposits through empirical methods (Ilstad et al. 2004; Færseth and Sætersmoen 2008).

The depth-averaged method (DAM) is arguably the approach used most frequently in industrial analysis of submarine landslides, in which the governing equations are simplified by averaging variables along the depth and then a shear layer and an overlying plug layer are assumed (Savage and Hutter 1991; Imran et al. 2001). The advantage of the DAM is that the three-dimensional and two-dimensional (2D) runouts are essentially simplified as 2D and one-dimensional (1D) problems, respectively. The DAM has been used for large scale events where shallow water approximations to the Navier-Stokes equations are accurate for

the overall behaviour of the runout, while the computational efficiency is attractive due to orders of magnitude less effort (Malet et al. 2004).

A variety of sliding patterns were observed in in-situ surveys and laboratory physical modelling (Hampton et al. 1996; Gue et al. 2010). Wang et al. (2011), Dong et al. (2017a) and Zhang et al. (2019) reported four runout mechanisms of submarine landslides found through numerical simulations, i.e. viscous elongation, block sliding, spreading of horsts and grabens and breakaway. Viscous elongation often appears in low-sensitivity material sliding along a relatively rough base, characterised with elongation of the slide in length and accordingly thinning in thickness. With the increasing basal friction due to expansion of the slide-base interface, the slide becomes stationary gradually. The block sliding, a mass keeps running for a very long distance, is formed when the shear strength of the slide is sufficiently high to cause trivial thinning in thickness and the basal friction is sufficiently low to allow for a lasting acceleration of the slide. The spreading of horsts and grabens is mainly induced by shear band propagation, with the materials inside the shear bands heavily remoulded. Breakaway mode represents departure of the front part of the slide from the main body, as the basal friction is relatively low.

The DAM solutions seem to be reasonable for slides with simple elongations (Jiang and LeBlond 1993; Imran et al. 2001), while it is not clear if the DAM can be used for complex morphologies as the sliding material might not be divided into the shear and plug layers (Pastor et al. 2009). For example, the DAM suffers from Riemann problem (Leveque 2002; Bernetti et al. 2008), which may cause wave breaking in slides. The scenarios of submarine landslides that can be simulated with the DAM are required to be defined for practical applications. Data for submarine slides show that the runout distances are two to three orders of magnitude larger than their subaerial counterparts in spite of increased viscous drag and reduced effective gravity due to buoyancy (Hampton et al. 1996; De Blasio et al. 2005). This phenomenon has been attributed to the frictional base with shear strength remarkably lower than the shear strength of the slide. Back-analysis of the first phase of the Storegga slide shows that the basal friction might be less than 0.5 kPa to reach the final runout distance although the intact shear strength of the sliding material is ranged in 50–100 kPa (De Blasio et al. 2005). Therefore, the conventional DAMs, which are specialised for no-slip base, also need to be enhanced to account for the frictional base.

Except for the DAMs, a number of novel numerical methods have emerged in recent decades to simulate the post-failure runout of submarine landslide within the frameworks of geomechanics or computational fluid dynamics (CFD; Iverson and Denlinger 2001; Luna et al. 2012), such as finite volume method (De Blasio et al. 2004; Gauer et al. 2005), smooth particle hydrodynamics (Pastor et al. 2009; Bonet and Kulasegaram 2000; Pasculli et al. 2013, 2014), large deformation finite element method (Wang et al. 2013; Dey et al. 2016) and most recently material point method (MPM) (Dong et al. 2017a, 2017b). Full governing equations, without assumption of layers along the depth, were solved in these approaches. The MPM is a novel approach located between the

finite element methods and the meshless methods, in which the sliding material is represented by Lagrangian particles and a fixed Eulerian mesh is used for calculations (Sulsky et al. 1995; Jassim et al. 2013; Soga et al. 2016). The particles carry all physical properties of the sliding material such as mass, volume, density, velocities, deformation gradient and stresses, whereas no permanent information on the mesh. Deformations of the sliding material can be derived by tracking the particles moving through the background mesh. Since the mesh is fixed in space, mesh entanglement in the conventional Lagrangian methods is avoided and the periodical remeshing and variable remapping are not required (Wang et al. 2013). The development of GPU parallel strategies (Dong et al. 2015; Dong and Grabe 2018) boosted the computation efficiency of the MPM.

The purpose of this paper is to assess the feasibility of the DAM for different sliding mechanisms in terms of runout distances and morphologies. An enhanced DAM is developed with a frictional base by considering the stability of the front and rear faces of the slide. The predictions of the enhanced DAM are compared with the MPM simulations. The ranges of the shear strength, viscosity and sensitivity parameters are investigated to determine the feasibility of the DAM, followed by discussion on different sliding patterns (e.g. elongation, block sliding, spreading of horsts and grabens and breakaway).

Methodology

Soil model

The mechanical behaviour of the sliding material is governed by rate effect and remoulding of strength, which can be considered by an enhanced Herschel-Bulkley (H-B) model (Einav and Randolph 2005; Boukpeti et al. 2012)

$$s_u = s_{uo} \left[1 + \eta \left(\frac{\dot{\gamma}}{\dot{\gamma}_{ref}} \right)^n \right] \left[\delta_{rem} + (1 - \delta_{rem}) e^{-3\xi/\xi_{95}} \right] \quad (1)$$

where s_u is the undrained shear strength of the sliding material, and s_{uo} is the threshold shear strength without rate effect and

$$U_j^{t+\Delta t} = U_j^t + \left[\frac{1}{D} \frac{\partial}{\partial x} \left(U^2 D + \frac{\alpha_1 - \alpha_2}{1 - \alpha_1} U_p^2 D - \frac{1 - \alpha_2}{1 - \alpha_1} U_p U D \right) - g \frac{\partial D}{\partial x} + g \sin \theta - \frac{1}{\rho D} s_{uo} \left(1 + \beta \eta \left| \frac{U_p}{\dot{\gamma}_{ref} D_s} \right|^n \right) \text{sgn}(U_p) \right] \Delta t \quad (3)$$

where D_s and D_p are the thicknesses of the shear layer and plug layer, respectively; D is the total thickness. ρ is the submerged density of the sliding material, g is the gravitational acceleration, θ is the slope angle, α_1 , α_2 and β are shape factors. Equations (2) and (3) are also applicable to rate-independent materials by considering $\eta = 0$ in Eq. (1).

(2) Enhanced DAM for frictional base

Essentially, the term $s_{uo} \left(1 + \beta \eta \left| \frac{U_p}{\dot{\gamma}_{ref} D_s} \right|^n \right)$ in Eq. (3) represents the resistance τ_b along the no-slip base. For a frictional base with a specific basal shear strength s_b , the basal resistance τ_b can be regulated by

remoulding. The first bracketed term of Eq. (1) represents the effect of strain rate characterised by the original H-B model: $\dot{\gamma}_{ref}$ is the reference shear strain rate, $\dot{\gamma}$ the shear strain rate, η the viscosity coefficient and n the shear-thinning index. With n and δ_{rem} taken as 1, Eq. (1) represents the Bingham model, which assumes a linear variation of the shear strength with shear strain rate. The second bracketed term of Eq. (1) represents the effect of remoulding: δ_{rem} is the strength ratio between fully remoulded and intact state (i.e. inverse of sensitivity S_t), and ξ is the cumulative plastic shear strain with ξ_{95} of the plastic shear strain required to achieve 95% of remoulding. For typical kaolin clays in deep waters, η and n are ranged in 0.3–0.7 and 0.1–0.4, respectively, with reference shear strain rate as 0.06 s^{-1} (Boukpeti et al. 2012). A typical value of δ_{rem} of kaolin used at the University of Western Australia is 0.25–0.7 (Sahdi et al. 2014), while the most extreme value for quick clays can be as low as 1/150 (Skempton and Northey 1952); the value of ξ_{95} often varies between 10 and 50 depending on the remoulding rate (Einav and Randolph 2005).

Algorithm of depth-averaged method

(1) Original DAM

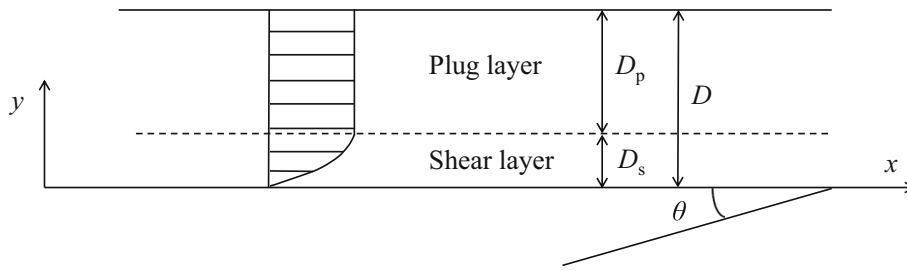
Almost all previous DAMs were specialised for insensitive material sliding down a rigid no-slip slope (Imran et al. 2001; see Fig. 1(a)), which is solved with a forward-difference Lagrangian method (Savage and Hutter 1991) by discretising the sliding material into a number of column elements (Fig. 1(b)). The plug layer velocity U_p and the averaged velocity U over the total thickness of node j at time $t + \Delta t$ are

$$U_{pj}^{t+\Delta t} = U_{pj}^t + \left[(U - U_p) \frac{\partial U_p}{\partial x} - g \frac{\partial D}{\partial x} + g \sin \theta - \frac{s_{uo}}{\rho D_p} \text{sgn}(U_p) \right] \Delta t \quad (2)$$

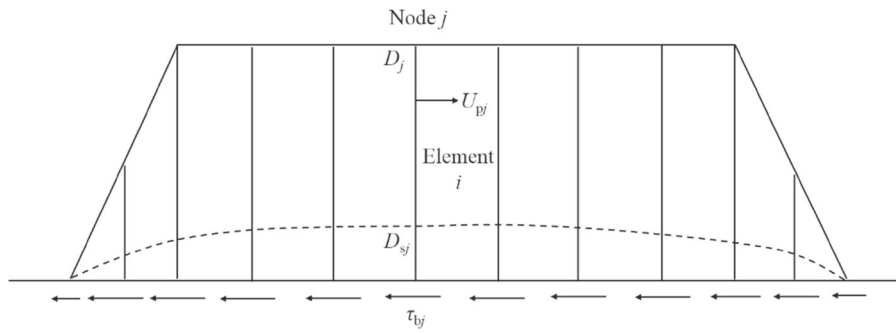
(3)

$$\begin{cases} \text{if } s_b \leq s_{uo}, \text{ no shear layer and } \tau_b = s_b \\ \text{if } s_{uo} < s_b \leq s_{uo} \left(1 + \beta \eta \left| \frac{U_p}{\dot{\gamma}_{ref} D_s} \right|^n \right), \tau_b = s_b \\ \text{if } s_{uo} \left(1 + \beta \eta \left| \frac{U_p}{\dot{\gamma}_{ref} D_s} \right|^n \right) < s_b, \text{ no-slip and } \tau_b = s_{uo} \left(1 + \beta \eta \left| \frac{U_p}{\dot{\gamma}_{ref} D_s} \right|^n \right) \end{cases} \quad (4)$$

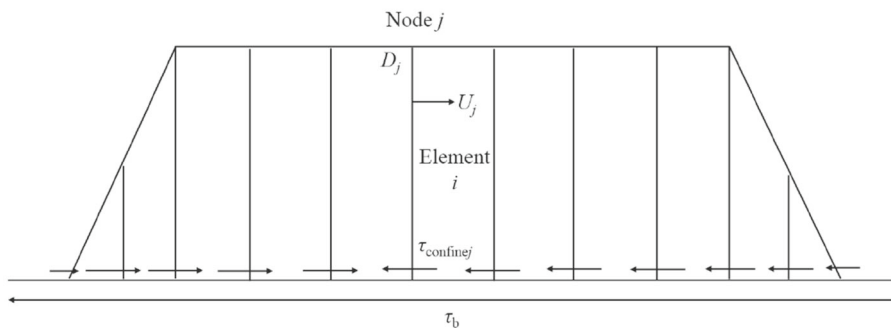
In the case of $s_{uo} \left(1 + \beta \eta \left| \frac{U_p}{\dot{\gamma}_{ref} D_s} \right|^n \right) < s_b$, the basal resistance τ_b defined by Eq. (4) follows the original DAM algorithm. In the case of $s_{uo} < s_b \leq s_{uo} \left(1 + \beta \eta \left| \frac{U_p}{\dot{\gamma}_{ref} D_s} \right|^n \right)$, the basal resistance τ_b is upper bounded by the basal shear strength s_b instead of the rate-dependent shear strength of the sliding material. In the case of $s_b \leq s_{uo}$, there is a plug layer only in the slide (Fig. 2) and the basal



(a) definition sketch of slide (after Huang and Garcia, 1997)



(b) discretisation of slide on no-slip base



(c) discretisation of slide on frictional base

Fig. 1 Simulation of submarine landslide with DAM. **a** Definition sketch of slide (after Huang and Garcia 1997); **b** discretisation of slide on no-slip base; **c** discretisation of slide on frictional base

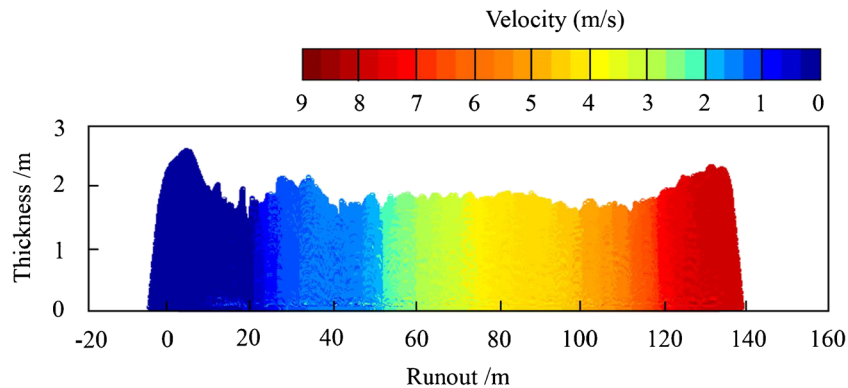


Fig. 2 Velocity contours predicted by MPM for a slide on frictional base ($s_{u0} = 2.5$ kPa, $s_b = 1$ kPa; Dong et al. 2017a)

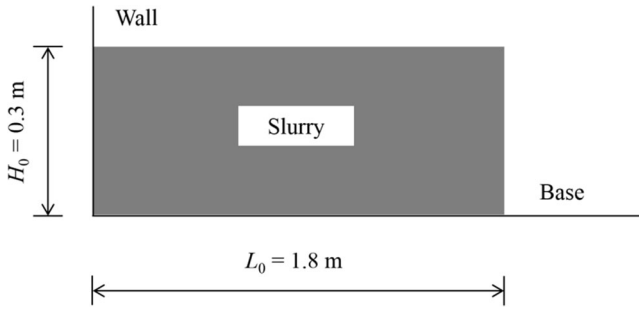


Fig. 3 GPU-hosted workstation for parallel computing

resistance τ_b is limited to the basal shear strength s_b , i.e. Eq. (3) is not required and s_{uo} in Eq. (2) needs to be replaced with s_b to account for the basal friction on the slide. However, the updated Eq. (2) ignores the shear strength of the sliding material, as a result, the slide tends to be over-stretched in length and over-thinned in thickness (Fig. 9), especially as s_b is much smaller than s_{uo} .

For an infinite length slide, the plug layer keeps slumping when gravitational driving force at the bottom is above the threshold shear strength of the material, which defines a critical thickness $H_{slump} = s_{uo}/\rho g \sin(\theta)$. Similarly, the front and rear faces of the finite length slide discussed here owns a critical thickness $H_{stability} = 4s_{uo}/\rho g$ for stability (Cai et al. 1990; Collins and Sitar 2011), which is equivalent to the effect of adding a virtual confining shear resistance at the base $\tau_{confiner} = 4\sin(\theta)s_{uo}$ (Fig. 1(c)). Then Eq. (4) is modified as

$$\begin{cases} \text{if } s_b \leq 4\sin(\theta)s_{uo}, \text{ no shear layer, } \tau_b = s_b \text{ and } \tau_{confiner} = 4\sin(\theta)s_{uo} \\ \text{if } 4\sin(\theta)s_{uo} < s_b \leq s_{uo}, \text{ no shear layer and } \tau_b = s_b \\ \text{if } s_{uo} < s_b \leq s_{uo} \left(1 + \beta\eta \left| \frac{U_p}{\gamma_{ref} D_s} \right|^n\right), \tau_b = s_b \\ \text{if } s_{uo} \left(1 + \beta\eta \left| \frac{U_p}{\gamma_{ref} D_s} \right|^n\right) < s_b, \text{ no-slip and } \tau_b = s_{uo} \left(1 + \beta\eta \left| \frac{U_p}{\gamma_{ref} D_s} \right|^n\right) \end{cases} \quad (5)$$

The stability of the front and rear faces is naturally considered for the case of $4\sin(\theta)s_{uo} < s_b$. To implement the virtual confining shear resistance in the DAM as $s_b \leq 4\sin(\theta)s_{uo}$, the movement of the slide is decomposed into two parts: (a) local slump under the gravitational driving force and the virtual confining shear resistance and (b) overall translation as a rigid body under the basal shear resistance. The virtual confining shear resistance is against the relative departure between different parts of the slide (see Fig.

1(c)), while the basal shear resistance is exerted on the whole. The mechanical prerequisite of the block sliding mode is that the thickness of the slide is larger than the critical thickness $H_{basal-friction} = s_b/\rho g \sin(\theta)$.

Validation with flume test

The DAM algorithm has been implemented in open-source software ‘BING’ by Imran et al. (2001), which was enhanced by improvements in terms of CPU parallelisation and allows for variable slide profiles. In the simulations using the DAM, the initial length b of each column element was $1/4000$ of the initial length of the slide L_0 . The time step was set as $0.001(b/g)^{0.5}$, where g is the acceleration of gravity, $g = 9.81 \text{ m/s}^2$.

The MPM analyses were undertaken using an in-house programme that stems from the open-source package Uintah (Guilkey et al. 2012). An enhanced contact algorithm ‘Geo-contact’ (Ma et al. 2014) and GPU parallel computing strategies (Dong et al. 2015; Dong and Grabe 2018) were incorporated into the programme. In all MPM simulations, a 4×4 particle configuration was allocated for each element fully occupied by particles prior to the calculation. The element size was selected as $\sim H_0/60$, which was sufficiently fine by trial calculations (Dong et al. 2017a). H_0 represents the initial height of the slide. Poisson’s ratio of the sliding material was taken as 0.49 to approximate constant volume under the undrained conditions. Young’s modulus was taken as $100s_{uo}$. The time step t was determined with a Courant number α of 0.3

$$\Delta t = \frac{\alpha d}{\sqrt{(\lambda + 2G)/\rho}} \quad (6)$$

where G and λ are the Lamé parameters.

To make a more comprehensive comparison, elongation of the H-B material along a no-slip base was also investigated with a CFD package ANSYS FLUENT (ANSYS 2011). In the CFD analysis, the sliding mass was regarded as an incompressible viscous fluid. The whole domain was discretised with quadrilateral elements, with minimum element size d_{min} of $\sim H_0/60$. The mesh was testified as sufficiently fine through trial calculations (Dong et al. 2017b). The sliding mass was considered to give rise to laminar flow using a ‘no-turbulence’ model. The pressure and velocity fields were computed with a scheme termed ‘pressure implicit with splitting of operator’. The time step in the explicit calculations was estimated by $t = \beta d_{min}/V$, where V is the velocity of the slide, the coefficient

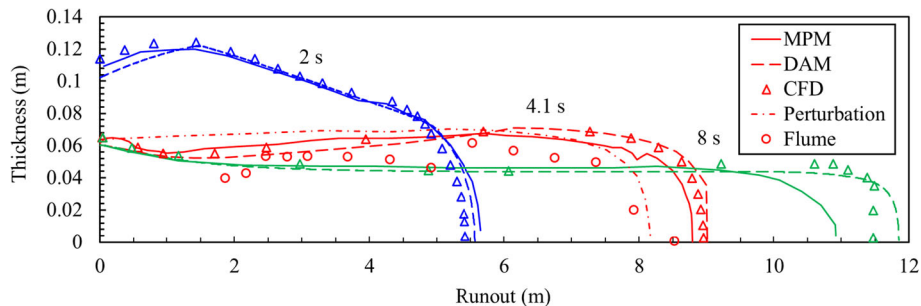


Fig. 4 Idealised geometry of dam break (not to scale)

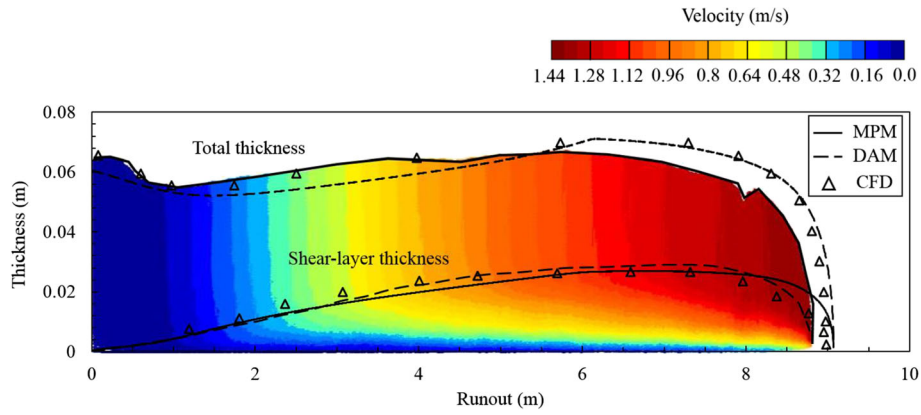
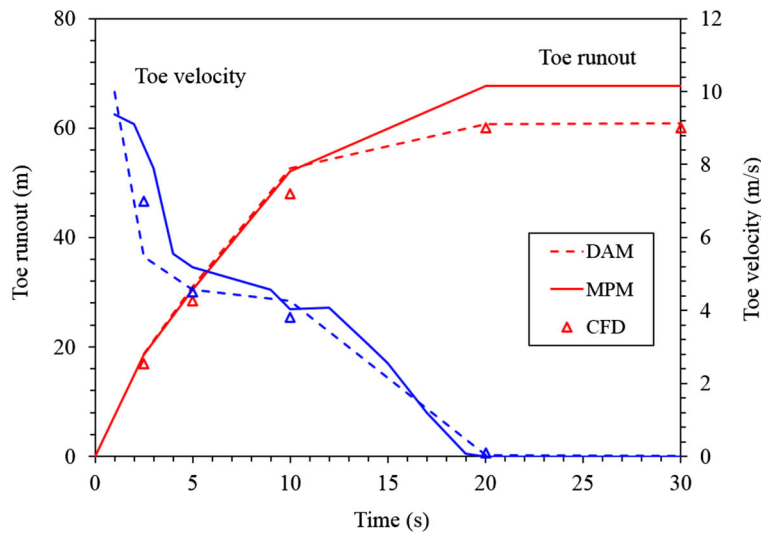


Fig. 5 Runout profiles of slurry flow

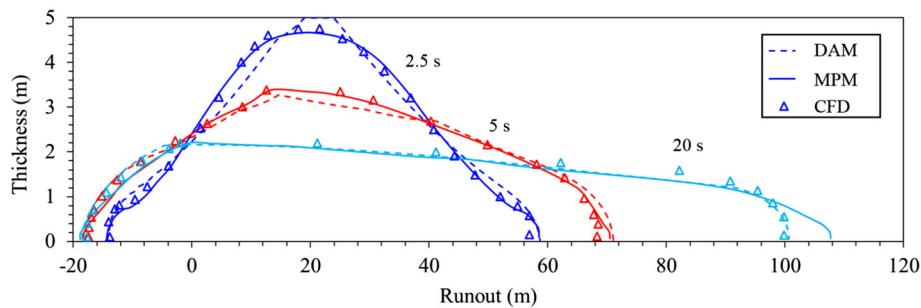
β was taken as 0.2. The MPM simulation was parallelised on a GPU NVIDIA Geforce Titan Xp featuring 3840 GPU cores (Fig. 3), while the DAM and CFD simulations were parallelised with 12 cores on CPU Intel i7-6850K.

A laboratory study of slurry runout induced by a dam break was carried out by Krone and Wright (1987) by instantaneously

releasing a bentonite slurry from an upstream reservoir into a rectangular flume. The test named 'Run 15' was modelled with the DAM, MPM and CFD, with initial configuration shown in Fig. 4. The base of the flume had an inclination of $\theta = 3.43^\circ$ to the horizontal. The initial length of the slurry was $L_o = 1.8$ m and the height $H_o = 0.3$ m. The density of the slurry was $\rho = 1073$ kg/m³.



(a) history of velocity and runout



(b) runout morphologies

Fig. 6 Shear layer thicknesses at 4.1 s

Table 1 Configuration of submarine landslide cases

Case	Base θ ($^{\circ}$)	Slide s_{uo} (kPa)	H	n	γ_{ref}	δ_{rem} ($1/S_1$)	ξ_{95}	Slide-base interface Boundary condition	s_b (kPa)	Runout DAM (m)	MPM	CFD	Runout mechanism
1	3.43	0.15	0.35	0.15	0.06	1	–	No-slip	–	284	300	310	Elongation
2	3.43	0.5	0.45	0.23	0.06	1	–	No-slip	–	62	68	60	Elongation
3	3.43	1	0.65	0.4	0.06	1	–	No-slip	–	19.7	19.7	19.4	Elongation
4	3.43	0.05	0.35	0.15	0.06	1	–	No-slip	–	1390	1163	–	Elongation
5	10	0.05	0.35	0.15	0.06	1	–	No-slip	–	4410	–	–	Elongation
6	5	5	0.45	0.23	0.06	1	–	No-slip	–	7.9	7.9	–	Elongation
7	5	5	0.45	0.23	0.06	1	–	Frictional	6	7.9	8.7	–	Elongation
8	5	5	0.45	0.23	0.06	1	–	Frictional	1.8	30	35	–	Elongation
9	5	5	0.45	0.23	0.06	1	–	Frictional	0.45	–	–	–	Block sliding
10	3.43	0.5	0.45	0.23	0.06	0.5	10	No-slip	–	125	134	–	Elongation
11	3.43	5	–	–	–	0.025	10	No-slip	–	–	–	–	Spreading
12	3.43	0.5	–	–	–	0.5	10	No-slip	–	–	–	–	Spreading
13	3.43	0.5	0.45	0.23	0.06	0.333	10	No-slip	–	141	158	–	Elongation

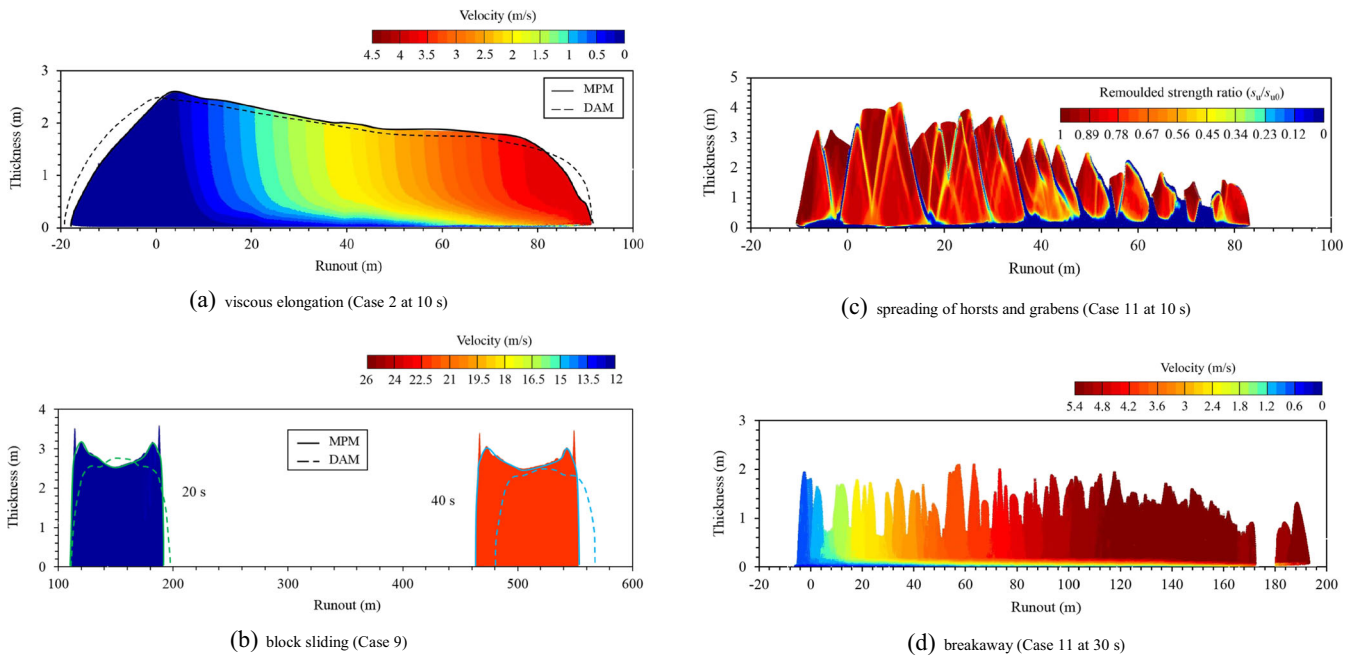


Fig. 7 History of mobility and morphologies of viscous slides in Case 2. **a** History of velocity and runout; **b** runout morphologies

The rheological behaviours of the slurry at the shear rates in the runout was approximated by a Bingham model with threshold shear strength $s_{uo} = 42.5$ Pa, and viscosity coefficient $\eta = 0.0052$. The base was assumed as no-slip, and the slurry-wall interface as frictional with a shear strength equivalent to s_{uo} (Krone and Wright 1987).

The runtimes for the DAM, MPM and CFD analyses were 1.2 h, 3.5 h and 96 h, respectively. For the MPM analysis, the solutions based on mesh sizes of $H_o/60$ and $H_o/120$ were nearly identical, indicating that the mesh size of $H_o/60$ was sufficiently fine. The runout profiles at 4.1 s predicted by all the numerical approaches agreed reasonably well with experimental observation (Krone and Wright 1987) and perturbation solution (Huang and García 1997), as shown in Fig. 5. The velocity contour at 4.1 s of the runout in the MPM analysis was shown in Fig. 6, from which the plug and shear layer can be distinguished clearly. The shear layer thicknesses predicted by the three approaches were close to each other.

Real-scale simulations

Viscous elongation

To investigate the real-scale slides, the initial length L_o and height H_o were increased to 40 m and 5 m, respectively, while the flume inclination remained as 3.43° . The wall boundary on the left side of the slide material was removed. The rheological behaviours of the slide were approximated with the H-B model (Eq. (1)). Three groups of threshold shear strength s_{uo} , viscosity coefficient η and shear-thinning index n were assumed for Cases 1–3 in Table 1, and the reference shear strain rate was remained as 0.06 s^{-1} . The submerged density of the sliding material was $\rho' = 600 \text{ kg/m}^3$.

Due to the variation of the threshold shear strengths and viscosities of the sliding materials, Case 1 is with a runout distance of ~ 300 m, compared with ~ 64 m for Case 2 and ~ 19.5 m for Case

3. The three numerical methods, DAM, MPM and CFD, have similar runout predictions (see Fig. 7(a)) with the divergence less than 13%, irrespective of model scales and material properties. Therefore, the depth-averaged simplification and the estimation of basal friction in the DAM are reasonable for the elongation of viscous slides on a no-slip base, and its predictions are reliable when compared with the non-averaged methods. The evolution of the slide morphologies predicted by the three approaches is also similar to each other as shown in Figs. 7(b) and 8(a) for Case 2. For lower shear strength cases, the DAM analysis may encounter computational instability induced by wave breaking termed as Riemann problem (Bernetti et al. 2008). Through trial calculations, the lowest shear strength of the sliding material to guarantee a stable DAM analysis is 0.05 kPa for the slope angle of 3.43° (Case 4) and 10° (Case 5). For Case 4, the runout distance by the MPM was 1163 m , 16% lower than the DAM solution. Due to the heavy computational effort, the CFD analyses for Cases 4 and 5 and MPM analysis for Case 5 were not completed.

Frictional base and block sliding

Cases 6–9 (Fig. 9) represent the comparison of no-slip and frictional bases. Case 6 is for a slide on a no-slip base, and the runout distance is as short as ~ 8 m. Cases 7–9 are for slides on frictional bases with a basal shear strength of 6 kPa , 1.8 kPa and 0.45 kPa , respectively, which are studied using the enhanced DAM (i.e. Eq. (5)). Case 7, with a basal shear strength $s_{uo} < s_b \leq s_{uo} \left(1 + \beta \eta \left| \frac{U_p}{\gamma_{ref} D_s} \right|^n\right)$, has a runout distance very close to that of Case 6 for the no-slip base. Case 8, with a basal shear strength $4 \sin(\theta) s_{uo} < s_b \leq s_{uo}$, provides a longer runout distance of ~ 32 m and more thinning in thickness than Cases 6 and 7; but the materials do not show overall translation. Case 9, with the basal shear strength further decreased to $s_b = 0.45 \text{ kPa}$ and in the range

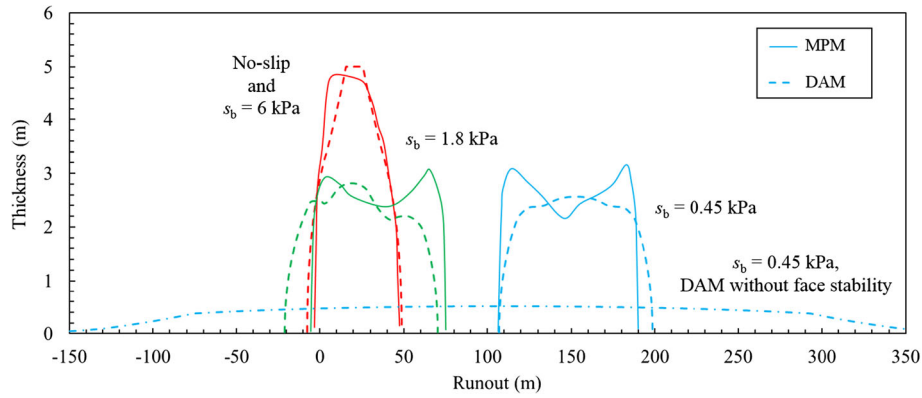
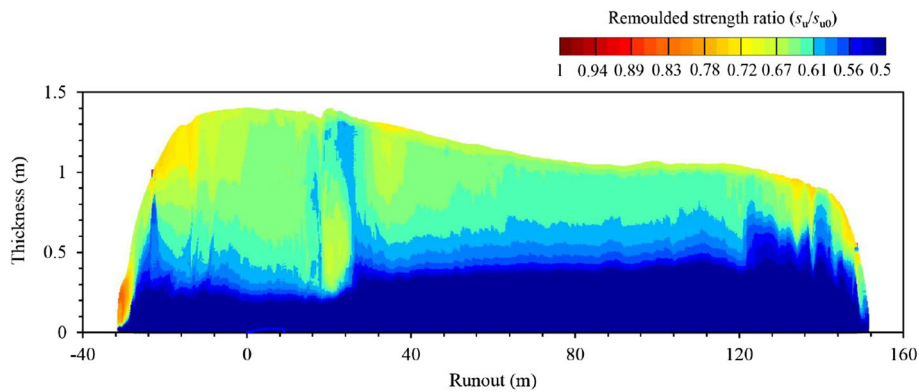


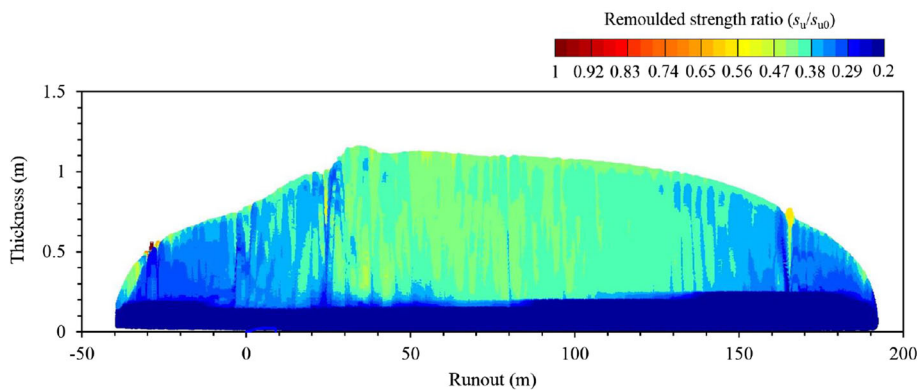
Fig. 8 Sliding mechanisms of submarine landslide. **a** Viscous elongation (Case 2 at 10 s); **b** block sliding (Case 9); **c** spreading of horsts and grabens (Case 11 at 10 s); **d** breakaway (Case 11 at 30 s)

$s_b \leq 4 \sin(\theta)s_{uo}$, is characterised with an obvious block sliding, approaching 200 m at 20 s. The slide keeps accelerating in Case 9, up to 12 m/s at 20 s (Fig. 8(b)), and will not stop. The height of the slides in Cases 8 and 9 remains ~ 3 m due to the stability of the front and rear faces as $H_{stability} = 3.4$ m. By comparing the morphology of Case 9 and those of Cases 6–8, it implies that the preconditions of block sliding: the shear strength of the slide is

sufficiently high to maintain a relatively high thickness of $4s_{uo}/\rho g$, and the basal friction is sufficiently low, $s_b \leq 4 \sin(\theta)s_{uo}$, to allow for a lasting acceleration of the slide. The runout distances and morphologies in Cases 6–9 predicted by the DAM analyses are close to that of the MPM simulations, which verifies the framework of the enhanced DAM for slides on frictional bases as in Eq. (5). The original framework without considering the stability of the



(a) viscous elongation in Case 10 at 20 s



(b) shear band along base in Case 12 at 20 s

Fig. 9 Morphologies for slides on frictional bases in Case 9

front and rear faces of the slide over-predicts the runout distance (350 m) as in Case 9 (Fig. 9).

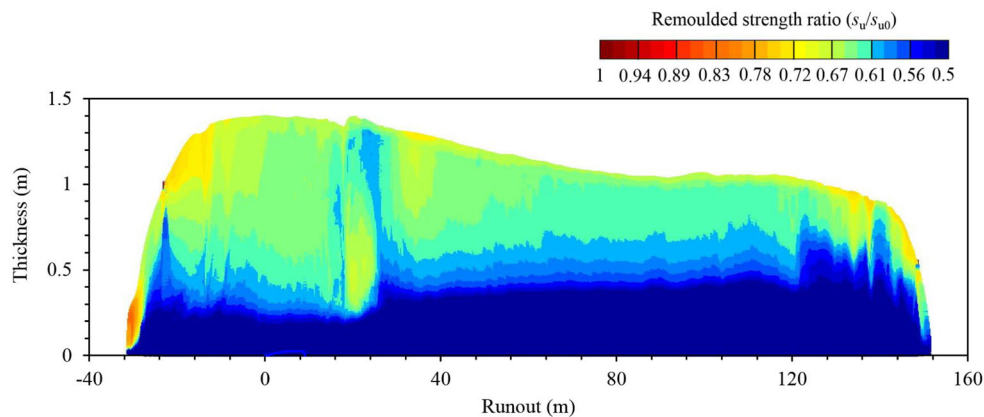
Spreading and breakaway

Case 10, similar to Case 2 but with a sensitivity of 2 rather than 1, is featured with runout distance of ~ 130 m larger than Case 2 due to the remoulding of the sliding material. The DAM and MPM analyses have similar predictions of the runout distances, and the runout morphologies of the slide remain viscous elongation. Most of the materials in the shear layer are fully remoulded while in the plug layer partially remoulded (Fig. 10(a)). The mobility of the slide is mainly determined by the remoulded strength in the shear layer.

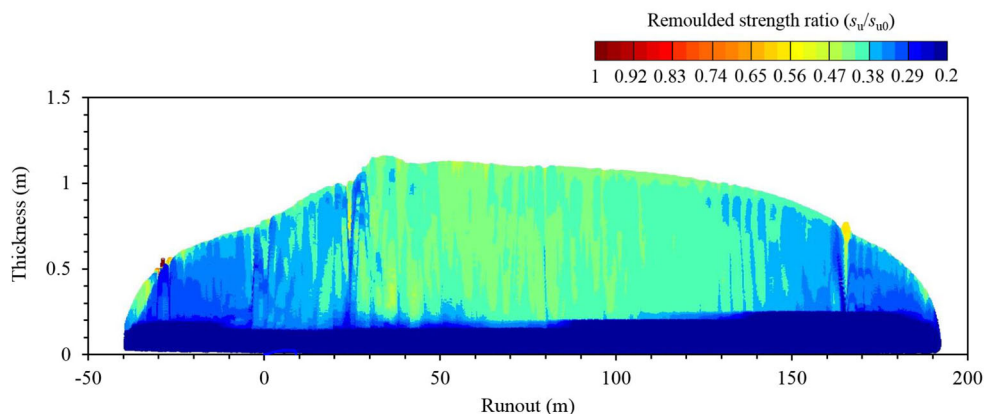
For sliding materials with a higher sensitivity, shear bands tend to form and propagate in the body of the slide, which are more complicated than viscous elongation (Dey et al. 2016; Puzrin et al. 2017). The DAM has no potential to capture the propagation of the shear bands in the plug layer, as a result, the runout distances and morphologies cannot be predicted accurately. To distinguish the viscous elongation for low-sensitivity materials and the shear band propagation for high-sensitivity materials and hence the feasibility of the DAM, the shear strengths and sensitivities of the slide are varied and the potential shear band propagations are investigated in the MPM analyses.

Soil sensitivities are selected as an extreme value of 40 (Skempton and Northey 1952) in Cases 11 and 2 in Case 12, respectively, while the rate-dependency effect is not considered. In Case 11, a series of horsts and grabens are formed with dislocation of the failed materials (Fig. 8(c)), which is caused by occurrence of shear bands. The heavily disturbed materials are localised inside the shear bands, while that in the wedge-shape grabens is disturbed slightly. The wedges tend to detach from each other due to velocity differences, as a result, the front wedges break away from the main body (Fig. 8(d)), which are expected to reach a very long runout distance as reported in Ilstad et al. (2004). Different from Case 10, shear band is mainly developed along the base in Case 12 (Fig. 10(b)). Through the comparison of the Cases 2, 10–12, it can be known that shear bands tend to be formed in sensitive materials when rate-dependency effect is not considered, and the DAM is not reasonable.

The strain rate-dependency effect has an opposite effect to that of remoulding, which means that the shear band propagation can be constrained, at least partially. By considering the rate parameters of $\eta = 0.45$ and $n = 0.23$ (Cases 10 and 13), no obvious shear band propagation is found for sliding materials with sensitivity $S_t \leq 3$; therefore, the morphologies of the slides remain viscous elongation and can be analysed with the DAM. In Case 13, the



(a) viscous elongation in Case 10 at 20 s



(b) shear band along base in Case 12 at 20 s

Fig. 10 Remoulded strength ratio in slides. **a** Viscous elongation in Case 10 at 20 s; **b** shear band along base in Case 12 at 20 s

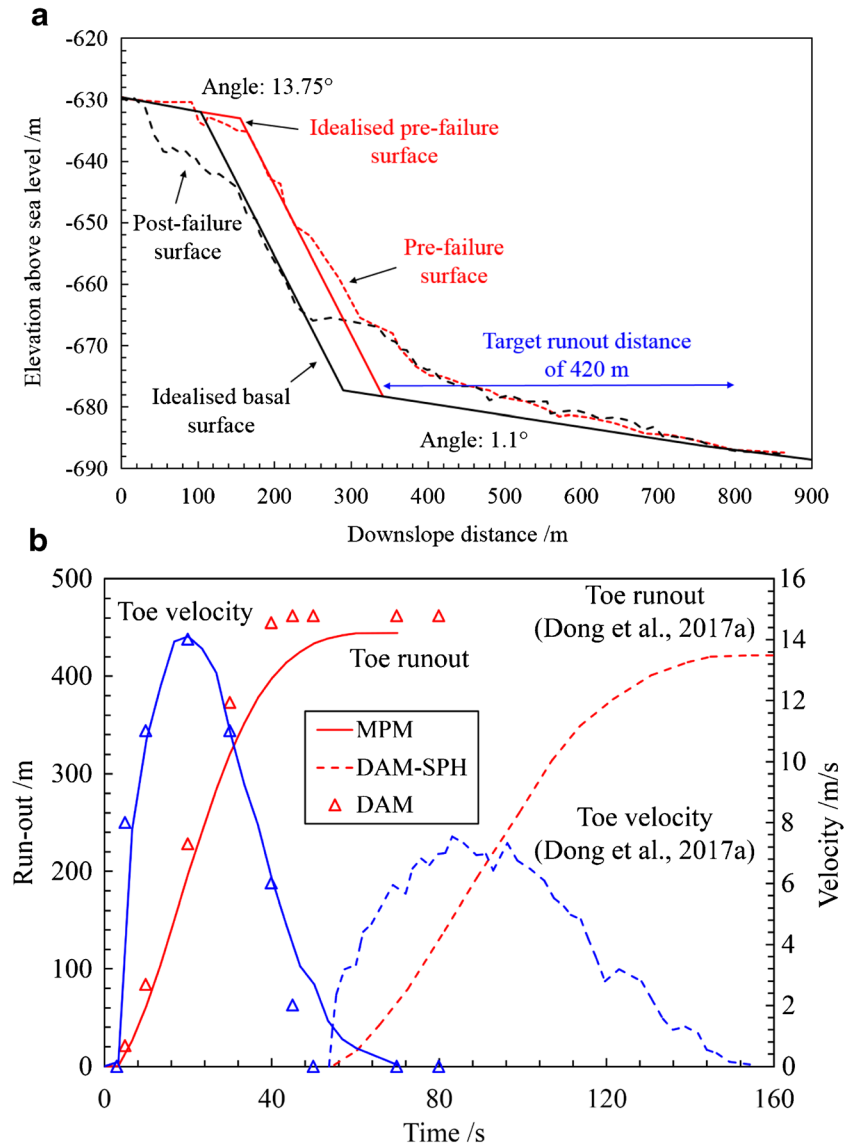


Fig. 11 Back-analysis of a southern Mediterranean slide. **a** Idealisation of slide transect; **b** history of toe velocity and runout

DAM analyses show similar predictions of runout distances to that of the MPM.

Back-analyses of real cases

A real case history of submarine escarpment failure in southern Mediterranean was back-analysed with the MPM and coupled DAM-SPH based on the post-failure bathymetric maps (Dong et al. 2017a). The profiles of the original and failed escarpments were surmised from the interpretation of the adjacent transect of the deposits, which implies that the failure was triggered by a steep slope and the runout on a gently inclined base reached a final distance of 420 m. Elevations of the idealised geometry are shown in Fig. 11(a). The slide was assumed to follow a viscous elongation mode and the slide-base interface was no-slip. The soil parameters were obtained through laboratory tests of soil samples retrieved from the field. The submerged density of the slide was 525 kg/m^3 . The soils were softening with the shear strength approximated

with Eq. (1), with $s_{u0} = 15 \text{ kPa}$, $\eta = 0.0167$, $n = 0.5$, $\gamma_{\text{ref}} = 1$, $\delta_{\text{rem}} = 0.025$ and $\xi_{95} = 45$. The original coupled DAM-SPH estimated the shear strain rate of each node with its velocity divided by the total thickness, which consequently under-estimates the accumulative shear strain and the softening effect. As a result, mobilisation of the slide simulated with the coupled DAM-SPH was delayed by 50 s (Fig. 11(b)), although the predicted final runout was close to the MPM prediction. Here, another calculation was performed with the DAM framework developed in this study, with the shear strain rate of each node calculated using its velocity divided by the shear layer thickness. In the DAM simulation, the slide is mobilised in 3 s after the startup of the calculation. The predicted final runout (462 m) is close to the MPM analysis (444 m) and the real scenario (420 m). The peak velocities predicted by the DAM analysis is similar to the MPM counterpart. Therefore, the DAM analysis can reasonably predict the dynamic behaviour of submarine landslide with viscous elongation mode.

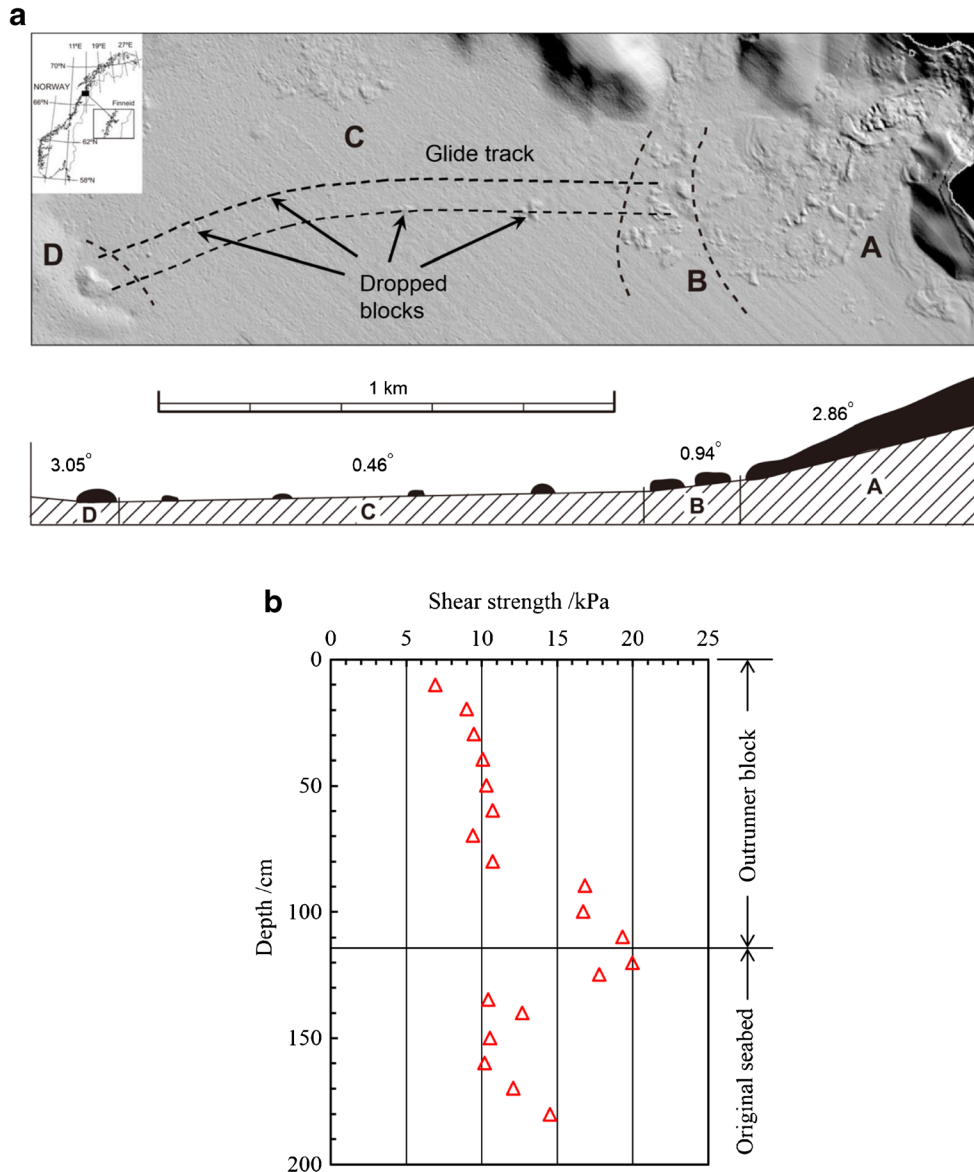


Fig. 12 Morphology and mechanical characteristics of Finneidfjord slide (after Ilstad et al. 2004). **a** Finneidfjord slide with morphology divided into four zones; **b** undrained shear strength of outrunner block and original seabed

Another shoreline slope failure occurred at the head of a fjord in northern Norway in 1996, mobilising about 1 million m³ of sediments. The depositing behaviour of the sediments and the environmental settings in the sliding area have been detailed by Best et al. (2003), Longva et al. (2003) and Ilstad et al. (2004). Investigations show that a series of slides were triggered by a weak layer accommodating free gas at about 6 m under the intact seabed sediment. The deposit of the largest event of the whole slides can be divided into four zones as shown in Fig. 12(a) (Ilstad et al. 2004). The main body of the deposit is in Zone A, which is within a distance of 1 km down the fjord and at an average slope angle of 2.86°. Beyond Zone A, blocks of soil were scattered in Zone B with an average slope angle of 0.94°, which are the departures from the main body similar to those shown in Fig. 8(d) for Case 11 in Table 1. Some blocks with higher mobility ran with long distances, and the largest block (110 × 60 × 2 m) stopped before the

flank of a moraine ridge located at Zone D. An obvious glide track with dropped blocks can be seen in Zone C with a very gentle slope of 0.46°. Earlier ground investigations showed that the sediments comprised soft sensitive clay with layers of quick clay and silt. Sensitivity of the quick clay generally varied from 5–35. Another coring programme was performed in 2001, in which undrained shear strength of the sediments were obtained by fall cone tests (Fig. 12(b); Ilstad et al. 2004). The undrained shear strength of the largest outrunner block increases from 7 kPa at the upper surface to 20 kPa at the bottom, while that for the original seabed varied between 10 and 15 kPa. Hydroplaning has been suggested as a mechanism for the long-distance transport of the outrunner blocks (Ilstad et al. 2004), which means that the water layer under the slide provides the basal resistance.

Back-analysis of the sliding process of the largest outrunner block is performed with the DAM and MPM. It is assumed that the plane block

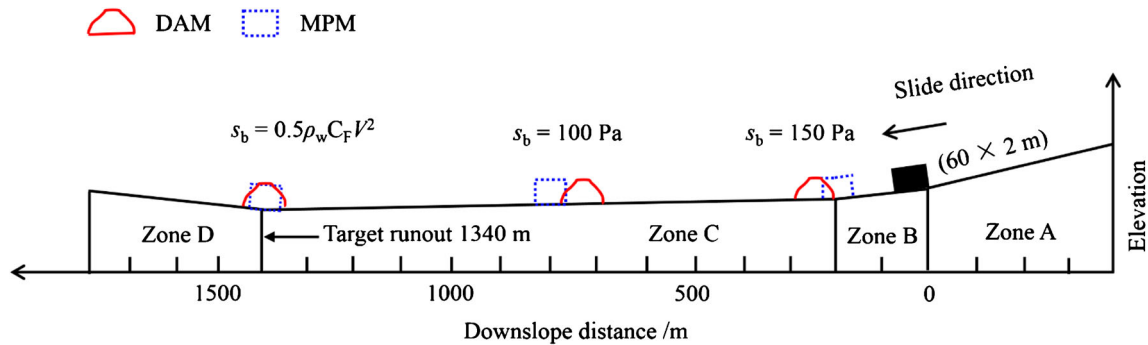


Fig. 13 Runout distances of block sliding with different basal resistances (exaggerated along vertical axis)

with dimensions of 60×2 m departs from the main body at the border of Zones A and B (Fig. 13), so the target runout is 1380 m. The submerged density of the slide was 500 kg/m^3 (Longva et al., 2003). The undrained shear strength of the homogeneous soil was 15 kPa. The interface between the slide and the rigid seabed (or water layer) was frictional. The preliminary analysis with static equilibrium shows that the block can be mobilised only if the resistance along the slide-seabed interface is lower than 161 Pa. The DAM and MPM analyses with consistent basal frictions but without hydroplaning show that the toe of the slide stops at a downslope distance of ~ 220 m and ~ 700 m for the basal resistance of 150 Pa and 100 Pa, respectively (Fig. 13). To achieve the target runout for the largest outrunner block at Zone D, the consistent basal resistance should be smaller than 60 Pa, which is much lower than the remoulded shear strength ($s_{uo} \geq 7 \text{ kPa}$ and $S_t \leq 35$) of the soils. This implies that the sensitivity behaviour of the soil is not sufficient to allow for a long runout along such gentle slopes. Another calculation was performed by considering the possible hydroplaning with a varying basal resistance of $s_b = 0.5\rho_w C_F V^2$ (De Blasio et al. 2004), where ρ_w is the density of water, C_F the drag coefficient and taken as 0.003 by De Blasio et al. (2004), and V the sliding velocity. Then, the predicted runouts are 1381 m by the DAM and 1400 m by the MPM, which are close to 1340 m as reported by Ilstad et al. (2004). In addition, the outrunner block finally stops at Zone D, as found in field investigation. The slide keeps accelerated in Zones B and C and the

highest toe velocity before Zone D is up to 7.2 m/s, which corresponds to a maximum basal friction of 78 Pa (Fig. 14). Therefore, hydroplaning proves to be the main reason for the long-distance runout of the block.

Conclusions

The feasibility of the depth-averaged method (DAM) for slides with different sliding modes was assessed in terms of runout distances and morphologies. The predictions by the DAM and material point method (MPM) agree well with that by experiments and computational fluid dynamics analyses for elongation modes. The conventional DAM algorithm specialised for no-slip bases was enhanced to reproduce the phenomenon of block sliding on frictional bases. The DAM fails to capture the spreading and breakaway modes due to the shear band propagation, which was reproduced with the MPM analyses. The ranges of the shear strength, viscosity and possible sensitivity parameters were determined for the feasible DAM analysis: the shear strength of the sliding material $s_{uo} \geq 0.05 \text{ kPa}$, and the sensitivity of the sliding material $S_t \leq 3$ for its strain rate-dependency parameters $\eta = 0.45$ and $n = 0.23$. Two real cases of submarine landslides, Southern Mediterranean slide and Finneidfjord slide, were back-analysed with the DAM and MPM. The sliding modes of viscous elongation and block sliding were reproduced.

Acknowledgements

Dr Spinewine Benoit from Fugro GeoConsulting and Dr Sam Ingarfield from Fugro AG. are acknowledged for kindly providing the geological information of the submarine landslide in southern Mediterranean and valuable suggestions in its back-analysis.

This work is also supported by NVIDIA Corporation with the donation of the GPU Geforce Titan Xp for this research.

References

- ANSYS (2011) ANSYS FLUENT 14.0 theory guide, ANSYS, Inc. v.14.0.1.
- Best AI, Clayton CRI, Longva O, Szuman M (2003) The role of free gas in the activation of submarine slides in Finneidfjord. In: Submarine mass movements and their consequences. Springer, Dordrecht, pp 491–498
- Bernetti R, Titarev VA, Toro EF (2008) Exact solution of the Riemann problem for the shallow water equations with discontinuous bottom geometry. J Comput Phys 227:3212–3243
- Bonet J, Kulasegaram S (2000) Correction and stabilization of smooth particle hydrodynamics methods with applications in metal forming simulations. Int J Numer Methods Eng 47(6):1189–1214

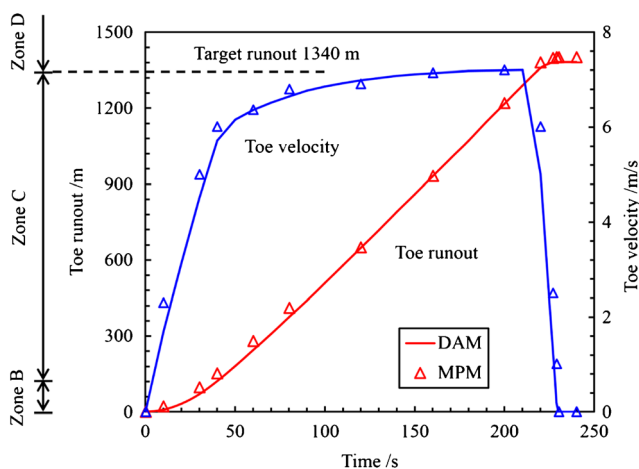


Fig. 14 History of toe velocity and runout by considering hydroplaning

- Boukpeti N, White DJ, Randolph MF, Low HE (2012) Strength of fine-grained soils at the solid-fluid transition. *Géotechnique* 62(3):213–226
- Bryn P, Berg K, Forsberg CF, Solheim A, Kvalstad TJ (2005) Explaining the Storegga slide. *Mar Pet Geol* 22(1–2):11–19
- Cai WM, Murti V, Valliappan S (1990) Slope stability analysis using fracture mechanics approach. *Theor Appl Fract Mech* 12(3):261–281
- Collins BD, Sitar N (2011) Stability of steep slopes in cemented sands. *J Geotech Geoenviron* 137:43–51
- De Blasio FV, Engvik L, Harbitz CB, Elverhøi A (2004) Hydroplaning and submarine debris flows. *J Geophys Res* 109(C1):1–15
- De Blasio FV, Elverhøi A, Issler D, Harbitz CB, Illstad T, Bryn P, Lien R (2005) On the dynamics of subaqueous clay rich gravity mass flows – the giant Storegga slide, Norway. *Mar Pet Geol* 22:179–186
- Dey R, Hawlader B, Phillips R, Soga K (2016) Numerical modeling of submarine landslides with sensitive clay layers. *Géotechnique* 66:454–468
- Dong Y, Grabe J (2018) Large scale parallelisation of the material point method with multiple GPUs. *Comput Geotech* 101:149–158
- Dong Y, Wang D, Randolph MF (2015) A GPU parallel computing strategy for the material point method. *Comput Geotech* 66:31–38
- Dong Y, Wang D, Randolph MF (2017a) Runout of submarine landslide simulated with material point method. In A Rohe, K Soga, H Teunissen & B Zuada Coelho (eds), *Procedia Engineering*, 175:357–364, 1st International Conference on the Material Point Method, Delft, Netherlands
- Dong Y, Wang D, Randolph MF (2017b) Investigating of impact forces on pipeline by submarine landslide using material point method. *Ocean Eng* 146:21–28
- Einav I, Randolph MF (2005) Combining upper bound and strain path methods for evaluating penetration resistance. *Int J Numer Methods Eng* 63(14):1991–2016
- Færseth RB, Sætersmoen BH (2008) Geometry of a major slump structure in the Storegga slide region offshore western Norway. *Nor Geol Tidsskr* 88(1):1–11
- Gauer P, Kvalstad TJ, Forsberg CF, Bryn P, Berg K (2005) The last phase of the Storegga Slide: simulation of retrogressive slide dynamics and comparison with slide-scar morphology. *Mar Pet Geol* 22(1):171–178
- Gue CS, Soga K, Bolton MD, Thusyanthan NI (2010) Centrifuge modelling of submarine landslide flows. In *Proceedings of the 7th International Conference on Physical Modelling in Geotechnics 2010, ICPMG 2010*, (2), pp 1113–1118
- Guilkey J, Harman T, Luitjens J et al (2012) Uintah code (Version 1.5.0). Computer program; available at <http://www.uintah.utah.edu>. Accessed 05.10.2015
- Hampton MA, Lee HJ, Locat J (1996) Submarine landslides. *Geophysics* 34(1):33–59
- Highland L, Peter TB (2008) *The landslide handbook: a guide to understanding landslides*. US Geological Survey, Reston
- Huang X, García MH (1997) A perturbation solution for Bingham-plastic mudflows. *J Hydraul Eng* 123(11):986–994
- Illstad T, De Blasio FV, Elverhøi A, Harbitz CB, Engvik L, Longva O, Marr JG (2004) On the frontal dynamics and morphology of submarine debris flows. *Mar Geol* 213(1):481–497
- Imran J, Harff P, Parker G (2001) A numerical model of submarine debris flow with graphical user interface. *Comput Geosci* 27(6):717–729
- Iverson RM, Denlinger RP (2001) Flow of variably fluidized granular masses across three-dimensional terrain: 1. Coulomb mixture theory. *J Geophys Res* 106:537–552
- Jassim I, Stolle D, Vermeer P (2013) Two-phase dynamic analysis by material point method. *Int J Numer Anal Methods Geomech* 37:2502–2522
- Jiang L, LeBlond PH (1993) Numerical modelling of an underwater Bingham plastic mudslide and the waves which it generates. *J Geophys Res* 98(C6):10,303–10,317
- Krone RB, Wright VG (1987) Laboratory and numerical study of mud and debris flow. In: Report 1 and 2 for Department of Civil Engineering. University of California, Davis
- Leveque RJ (2002) *Finite volume methods for hyperbolic problems*. Cambridge University Press, Cambridge
- Leynaud D, Sultan N, Mienert J (2007) The role of sedimentation rate and permeability in the slope stability of the formerly glaciated Norwegian continental margin: the Storegga slide model. *Landslides* 4:297–309
- Locat J, Lee HJ (2005) Subaqueous debris flows. In: *Debris-flow hazards and related phenomena*. Springer, Berlin Heidelberg, pp 203–245
- Longva O, Janbu N, Blikra LH, Bøe R (2003) The 1996 Finneidfjord slide seafloor failure and slide dynamics. In: *Submarine mass movements and their consequences*. Springer, Dordrecht, pp 531–538
- Luna BQ, Rémaitre A, van Asch TWJ, Malet JP, van Westen CJ (2012) Analysis of debris flow behavior with a one dimensional run-out model incorporating entrainment. *Eng Geol* 128:63–75
- Ma J, Wang D, Randolph MF (2014) A new contact algorithm in the material point method for geotechnical simulations. *Int J Numer Anal Methods Geomech* 38(11):1197–1210
- Malet JP, Maquaire O, Locat J, Rémaitre A (2004) Assessing debris flow hazards associated with slow moving landslides: methodology and numerical analyses. *Landslides* 1:83–90
- Norem H, Locat J, Schieldrop B (1990) An approach to the physics and the modelling of submarine landslides. *Mar Georesour Geotechnol* 9:93–111
- Pasculli A, Minatti L, Sciarra N, Paris E (2013) SPH modeling of fast muddy debris flow: numerical and experimental comparison of certain commonly utilized approaches. *Ital J Geosci* 132(3):350–365
- Pasculli A, Minatti L, Sciarra N (2014) Insights on the application of some current SPH approaches for the study of muddy debris flow: numerical and experimental comparison. *Proceedings of 10th International Conference on Advances in Fluid Mechanics, A Coruña, Spain*, 82, pp 3–14
- Pastor M, Haddad B, Sorbino G, Cuomo S, Drempetic V (2009) A depth-integrated, coupled SPH model for flow-like landslides and related phenomena. *Int J Numer Anal Methods Geomech* 33:143–172
- Puzrin AM, Gray TE, Hill AJ (2017) Retrogressive shear band propagation and spreading failure criteria for submarine landslides. *Géotechnique* 67(2):95–105
- Sahdi F, Gaudin C, White DJ (2014) Strength properties of ultra-soft kaolin. *Can Geotech J* 51:420–431
- Savage SV, Hutter K (1991) The dynamics of avalanches of granular materials from initiation to runout. Part 1: analysis. *Acta Mech* 86:201–223
- Skempton AW, Northey RD (1952) The sensitivity of clays. *Géotechnique* 3(1):30–53
- Soga K, Alonso E, Yerro A, Kumar K, Bandara S (2016) Trends in large-deformation analysis of landslide mass movements with particular emphasis on the material point method. *Géotechnique* 66(3):1–26
- Sulsky D, Zhou SJ, Schreyer HL (1995) Application of a particle-in-cell method to solid mechanics. *Comput Phys Commun* 87(1):236–252
- Wang D, Randolph MF, White DJ (2011) A parametric study of submarine debris flows using large deformation finite element analysis. The VI report for the JIP project modelling of submarine slides and their impact on pipelines from Minerals and Energy Research Institute of Western Australia, Project No. M395
- Wang D, Randolph MF, White DJ (2013) A dynamic large deformation finite element method based on mesh regeneration. *Comput Geotech* 54:192–201
- Zhang W, Randolph MF, Puzrin AM, Wang D (2019) Transition from shear band propagation to global slab failure in submarine landslides. *Can Geotech J* in press

Y. Dong

College of Marine Science and Technology,
China University of Geosciences,
388 Lumo Road, Wuhan, 430074, China
Email: dongyk@cug.edu.cn

Y. Dong

Shenzhen Research Institute,
China University of Geosciences,
Shenzhen, 518057, China

D. Wang

Shandong Provincial Key Laboratory of Marine Environment and Geological Engineering,
Ocean University of China,
238 Songling Street, Qingdao, 266100, China
e-mail: dongwang@ouc.edu.cn

L. Cui

State Key Laboratory of Geomechanics and Geotechnical Engineering, Institute of Rock and Soil Mechanics,
Chinese Academy of Sciences,
Wuhan, 430071, China
e-mail: lcui@whrsm.ac.cn